

Black phosphorene tune electronic properties via directional C-doped

Renan N. Pedrosa,^{*a} Wanderlã L. Scopel,^a and Rodrigo G. Amorim^b

The tuning black phosphorene properties such as structural, electronic, transport are explored via substitutional C-doped. We employed density functional theory (DFT) calculations in combination with non-equilibrium Green's function (NEGF) for modeling the systems. Our results revealed that substitutional C-doped phosphorene are energetically favorable, and ruled by exothermic process. We also found that C-doping induces a change of the electric properties, such as a semiconductor-to-metal transition for the most lower concentration and *zig-zag* C-wire. Moreover, for an *armchair* C-wire and the most higher concentration the semiconductor character is kept, meanwhile the direct-to-indirect transition is observed to band gap nature. Finally, we show that there exist a dependence of the electronic transport with directional character of the C-doped configuration, and the possibility to control the local electric current probability through the applied gate voltage. The C-doped phosphorene findings demonstrated that, the direction play the role for conductance on 2D platform.

Since the isolation of graphene in 2014, there is a great interest in two-dimensional (2D) materials for applications as new platform for atomically thin devices. The 2D-material composed of atomic layers have received enormous attention due to unusual fascinating properties and its great potential for applications such as electronic, mechanics, electronic transport, sensing and optoelectronic. There are various ways to manipulate the physical properties of the 2D materials such as: the substitutional defects¹, vacancies^{2,3}, strain^{4,5}, topological defects line⁶ and molecules adsorption^{7,8}.

Among 2D materials, a single-layer of the phosphorus (phosphorene) has received enormous attention, after its successful exfoliation by Liu *et al.*⁹. Even though, there are many allotropes of the elemental phosphorus, the most stable form among them is the black phosphorus. The phosphorene, has a puckered honeycomb structure that present intriguing electronic properties, such as: high carrier mobility¹⁰, high anisotropic properties¹¹, and band gap as a function of the numbers of layers¹². Furthermore, it is well know that the phosphorene sheet is very sensitive to environment molecules^{13,14}.

The atomically-precise structural modification of the phosphorene sheet are very desirable to control its electronic properties. Due to the extraordinary control over the electronic properties of

the phosphorene nanoribbon^{15–18}, in 2019, Mitchell *et al.*¹⁹ have successfully synthesized an individual phosphorene nanoribbon with high-quality and aligned exclusively along *zig-zag* direction. Moreover, lateral²⁰ and vertical²¹ phosphorene-graphene heterostructures, and vertical Phosphorene/hBN interface has been explored²², as well as the transition metal²³ and substitutional doped phosphorene^{8,24}. In this context, a better understanding of the C doping with different concentrations and geometry configurations are open issues.

Our investigation focuses on the structural and electronic properties, electronic transport properties and energetic stability of substitutional carbon atoms in the phosphorene through the total energy calculations based on the Density Functional Theory (DFT). The C-doped phosphorene for different structural configurations and concentrations were investigated. Ours results finding that for all different doping configurations considered herein, the defects formation is ruled by exothermic processes. The energetic stability revealed that the most stable configurations were 2.35 eV/atom and 2.36 eV/atom. Furthermore, C doped phosphorene for specific configurations induced the transition of the direct to indirect gap and another configurations, the tuning of the semiconductor to metallic character was observed. Finally, we verified that the high directional character of the electronic and transport properties for C-line *zig-zag* compared to armchair interface.

1 Method

The total energy calculation were performed within the density functional theory (DFT), where the exchange-correlation term was described within the generalized gradient approximation as

^a Departamento de Física, Universidade Federal do Espírito Santo- UFES , Vitória/ES, Brazil; E-mail: renannarcisopedrosa@gmail.com

^a Departamento de Física, Universidade Federal do Espírito Santo- UFES , Vitória/ES, Brazil; E-mail: wanderla.scopel@ufes.br

^b Departamento de Física, ICEx, Universidade Federal Fluminense - UFF, Volta Redonda/RJ, Brazil; E-mail: rgamorim@id.uff.br

proposed by Perdew, Burke and Ernzerhof (GGA-PBE)²⁵. The electron-ion interactions are taken into account using the Projector Augmented Wave (PAW) method²⁶. The calculations of the equilibrium geometries, total energies, and the electronic band structures were done by using the VASP code^{27,28}. The Kohn-Sham orbitals are expanded in a plane wave basis set with an energy cutoff of 550 eV. The 2D Brillouin Zone (BZ) is sampled according to the Monkhorst-Pack method²⁹, using a gamma-centered $6 \times 6 \times 1$ mesh. We have also used a $3 \times 4 \times 1$ phosphorene supercell and the geometries have been relaxed until atomic forces were lower than 0.025 eV/Å. The optimized lattice parameter of the black phosphorene was $a = 4.51$ and $b = 3.30$ Å.

The electronic transport calculations were performed via the non-equilibrium Green's function (NEGF) formalism using the DFT Hamiltonian, as implemented in the TranSiesta^{30,31} code. The Kohn-Sham (KS) orbitals were expanded in a linear combination of numerical pseudo-atomic orbitals using split-valence double-zeta basis set including polarization functions^{32,33}, and the kpoint grid of $1 \times 1 \times 128(1 \times 1 \times 1)$, for electrode (scattering) region. The electronic transport setup was build considering the z -axis as the transport direction. For transport models, an important quantity consists of the electrons transmission ($T(E)$), for a given energy E . The physical meaning of it is, for a specific energy E an electron from the left electrode may reach the right one, passing through the scattering region. The transmission is given by:

$$T(E) = \text{Tr} \left[\Gamma_R(E) G^R(E) \Gamma_L(E) G^A(E) \right], \quad (1)$$

where $\Gamma_{L,R}(E)$ is the coupling matrix, related with the left and right electrodes and $G^{R,A}$ is the retarded (advanced) Green function. The transmission is related to the quantum conductance as well as the electronic current. Then, for zero-bias calculations the transmission could be projected in Real Space. This projection gives the local current³⁴, expressed using the Keldysh formalism³⁵ in which the current density between two sites M and N is given by:

$$i(E)_{N \rightarrow M} = 4 \frac{e}{h} \sum_{\substack{n \in N \\ m \in M}} \Im \left[\left\{ \mathcal{G}(E) \Gamma_L \mathcal{G}^\dagger(E) \right\}_{mn} H_{nm} \right], \quad (2)$$

the spectral function ($\mathcal{G}(E) \Gamma_L \mathcal{G}^\dagger(E)$) and the Hamiltonian elements H_{nm} are represented, where the sum runs over all localized atomic orbitals n and m of the basis set. This are associated with N and M sites, respectively.

2 Results

In Figures 1 a-f we depicted the fully relaxed atomic geometries for pristine and C-doped 2D-phosphorene. Pristine black phosphorene, formed by a puckered structure with two layers separated by 2.12 Å, is presented in Figure 1 a. We can also note that there are three P-P bonds, which are not at the same plane, with

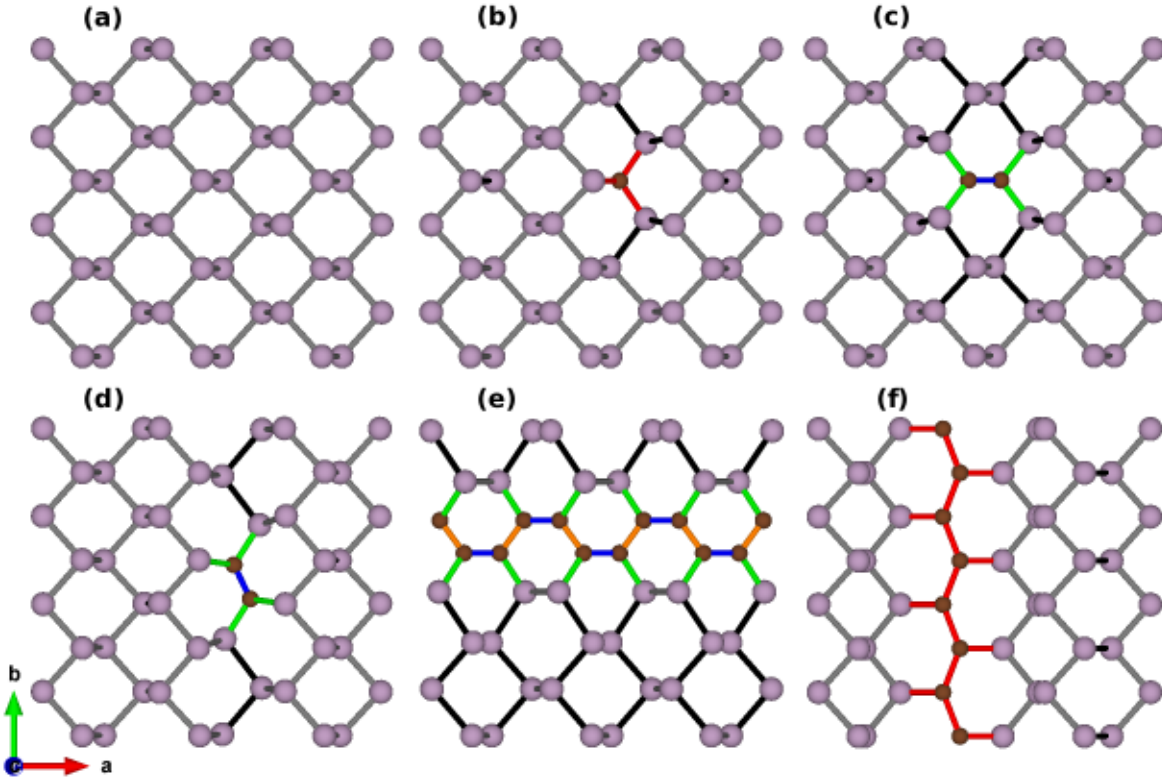


Fig. 1 The fully relaxed geometries are shown, where the light pink ball (smaller brown) sphere represent the P(C) atoms. The panel (a) represents the pristine Phosphorene. We are considering BP- n_c , where n_c is the number of Carbon atoms in the supercell. For BP-2C we have two configurations: i) p index represents C-doped parallel to a axis; ii) t index means C-doped tilted to a axis. The panels represent (b) BP-1C; (c) BP-2C-p; (d) BP-2C-t; (e) BP-12C; (f) BP-8C.

length ranges from 2.19 to 2.26 Å (represented by gray color) depending on the local environment, in agreement with previous studies³⁶.

To get some insights on the atomic deformations of the different n_C in the phosphorene, Figure 1-b-f show the C-doped phosphorene for n_C from 1 up to 12, where P atoms were replaced by C atoms. From relaxed geometries we noted that the C-doped induces local distortions on the structures, where the P-P bond length range from 2.26-2.33 Å (represented by black color), compared to pristine P-P bonds (gray color). More specifically, in Figure 1-b, the C atom is three coordinate with P atoms and the P-C bonds range from 1.77 up to 1.81 Å (red color), in accordance with the literature⁸.

Figures 1c-d show different atomic geometries configurations for $n_C=2$. The c-doped lead to the changes of the interatomic distance of the P-P bonds (black color) on both configurations, as already verified to $n_C=1$ configuration. Furthermore, we also note that the C-C bond length range from 1.38-1.42 Å (blue color) and C-P ranges from 1.86-1.84 Å (green color). It is worth noting that increasing n_C from 1→2, there is an increases of the C-P bonds from red to green color.

Figures 1e-f show a C-wire at *armchair* and *zig-zag* configurations in the phosphorene, respectively. As per shown in Figure 1-e one can observed a striped composed by C atoms with *armchair* geometry, whereas there are C-C bonds length in the two interatomic distance ranges 1.38-1.43 (blue color) and 1.52-1.53 (orange color). It was also determined that C-P bond length range from 1.86-1.84 Å (green color). However, the P-P bonds are at black color, which interatomic distance is higher than pristine P-P bonds (gray color). For the last configuration studied herein, Fig-

ure 1-f shows a C-wire at *zig-zag* configuration, where C-C bonds is represent by red color, showing the same interatomic distance of the Figure 1b. Overall, the P-P bonds represented by black color are always present in the C-doped phosphorene, showing that C induces a structure distortion in the black phosphorene.

Next, we examine the energetic stability of the C-doped phosphorene. The formation energy were determined for different C-doping concentrations and configurations, using the following equation:

$$E_{form} = E(BP_{doped}) - [n_P \mu_P + n_C \mu_C] \quad (3)$$

where $E(BP_{doped})$ is the total energy for different C-doping, μ_P (μ_C) is energy per phosphorus atom in a perfect phosphorene sheet (the energy per carbon atom in a perfect graphene sheet). The n_C is number of carbon atoms, and $n_P = N - n_C$ the number of the P atoms in the supercell, whereas N is the total number of the atoms in the supercell. The formation energy of the C-doping for each configuration studied is summarized in Table 1.

Table 1 The formation energy in eV/atom of C-doped black phosphorene.

n_C	Geometry	E_{form}
1	BP-1C	-1.73
2	BP-2C-p	-2.36
2	BP-2C-t	-1.80
8	BP-8C	-0.86
12	BP-12C	-2.35

The Table 1 shows the formation energy for C-doped and we can note that BP-2C-p and BP-12C geometries are the most ener-

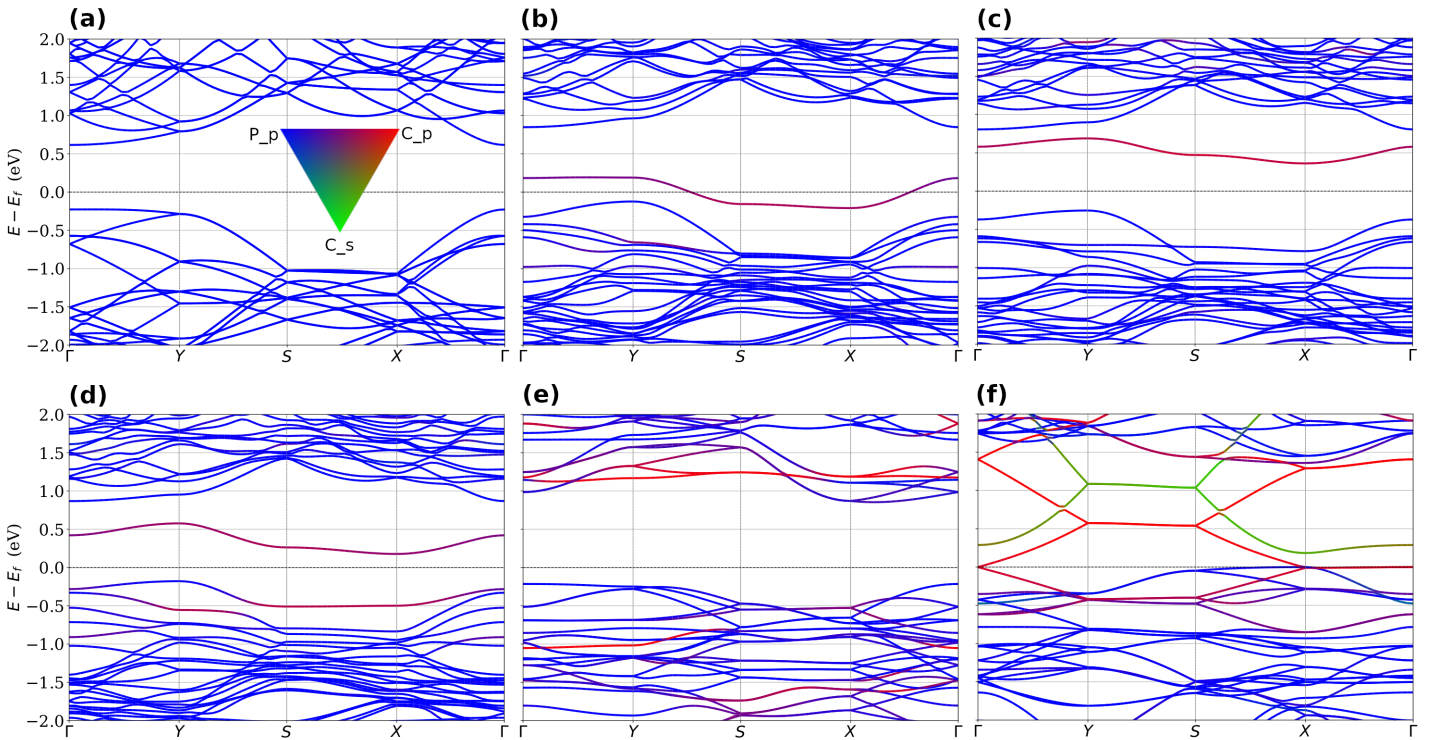


Fig. 2 Projected band structure (a) pristine phosphorene; (b) BP-1C; (c) BP-2C-p; (d) BP-2C-t; (e) BP-12C; (f) BP-8C.

getically stable configurations with -2.36 eV/atom. However, the BP-8C configuration is the least stable of them. Nevertheless, the energy formation of the BP-1C (BP-2C-t) configuration is -1.73 (-1.80 eV). Our finding revealed that the C-doping formation in the black phosphorene is governed by an exothermic process, in good agreement with previous data³⁷.

Figure 2 shows the projected band structure of the pristine phosphorene and C-doped phosphorene (see Figures 1). In particular, Figure 2-a shows that conduction (CB) and valence band (VB) are mostly due to the P- p orbitals (blue color) and a semiconductor character of the pristine phosphorene with direct band gap ($E_g=0.79$ eV), in good accordance with the literature⁹.

In order to explore the effect of the C-doped on the electronic structure of the phosphorene, we calculated the projected band structure as shown in Figures 2b-d. More specifically, Figure 2b shows the projected band structure for the case where we replaced one P atom by C, i.e., $n_C = 1$. From it, we can observe an emergence of a band (mixture of the blue and red colors), which is associated with p -hybridization between C and P atoms. In S-X path one observe highest contribution coming from C_p . It is worth noting that the band emerged is crossing the Fermi level, indicating a metallic character for a C-doped, in agreement with previous works^{8,37}.

Figures 2c-d shows the projected band structure for $n_C = 2$, but for different configurations such as: (i) BP-2C-p and (ii) BP-2C-t. It is observed for (i) and (ii) a band (mixture of the red and blue colors) emerge above the Fermi level in the energy range

0.25 up to 0.75 eV with a similar topology and both configurations present a semiconductor character. We also note that an increase of the n_C from $0 \rightarrow 2$ induces a transition in the nature of the band gap from direct-to-indirect. However, for the case (i) this band at X-point is 0.36 eV above E_f with an indirect $E_g = 0.54$ eV (Y-X direction), where in the case (ii) the band at X-point is located 0.15 eV above E_f with a $E_g = 0.27$ eV. It is important to emphasize that from (i) \rightarrow (ii) there is an increase of the contribution of the C- p_z and P- p_z orbitals and energy wide due to P-C bonds compared to (i), leading to an increase in the dispersion of that band. For case (ii), we can also verify the emergence of the new band at S- Γ -direction below of the Fermi level, which is attributed to a strong hybridization between C- p_z and C- p_x at lower energy compared to case (i).

Regarding C-doped in form of C-wire in the black phosphorene, we have considered *armchair* (BP-12C) and *zigzag* (BP-8C) configurations, as showed in the Figs. 1e-f, respectively. Figures 2e-f show that the *armchair* and *zigzag* configurations present features of the semiconductor and metallic character, respectively. For the *armchair* configuration one also observed that the nature of the band gap is indirect ($\Gamma \rightarrow X$ path) with $E_g = 0.99$ eV. The CBM is associated to the p_x orbitals of P atoms around the C line (blue color), whereas that the band (red color) strongly localized around 1.1 eV above E_f is ascribed to p_z orbitals of the C line. For the case BP-8C we can note a metallic character, once there are bands crossing the Fermi level. In addition, the bands crossing the Fermi level along the Γ -Y and S-X directions (below and

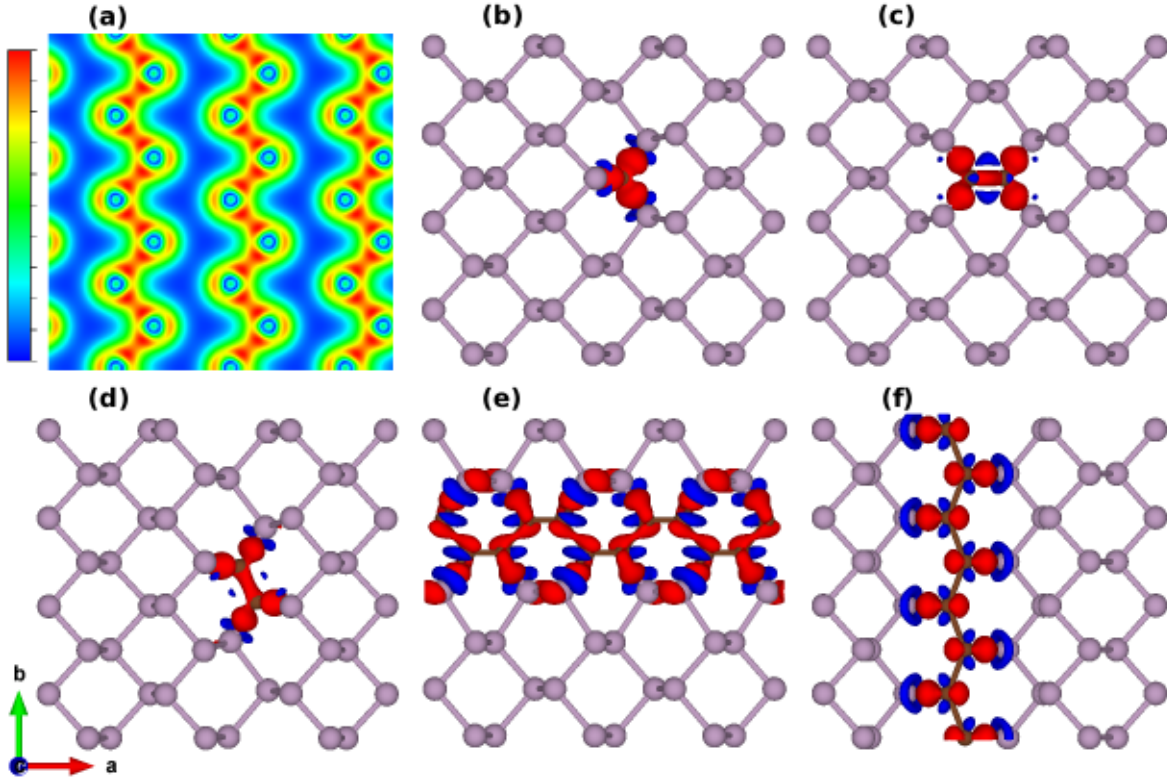


Fig. 3 (a) pristine phosphorene sheet (0.000 (blue)-0.127 e/Å³ (red)) and (b-f) C-doped phosphorene sheet. The red(blue) color represent positive(negative) values. $\Delta\rho(\vec{r}) > 0$ and $\Delta\rho(\vec{r}) < 0$ are represented by red and blue colors, respectively. Isosurface 0.0105 e/Å³

above E_f) we can note a linear dispersion mostly ascribed to p_z and p_x orbitals of the C line, whereas at E_f we see dispersionless in the S-X direction due to P- p_z contribution. As we see in the X- Γ direction there is a dispersionless at E_f , mostly composed by C- p_z and C- p_x orbitals. However, in the Y-S-X direction we can see a dispersion band centered at S direction mostly contribution becoming from P- p_z . Then, for the C-wire configurations we verified the high anisotropic character of the electronic properties, which indicating that the electronic properties present a strong direction dependence.

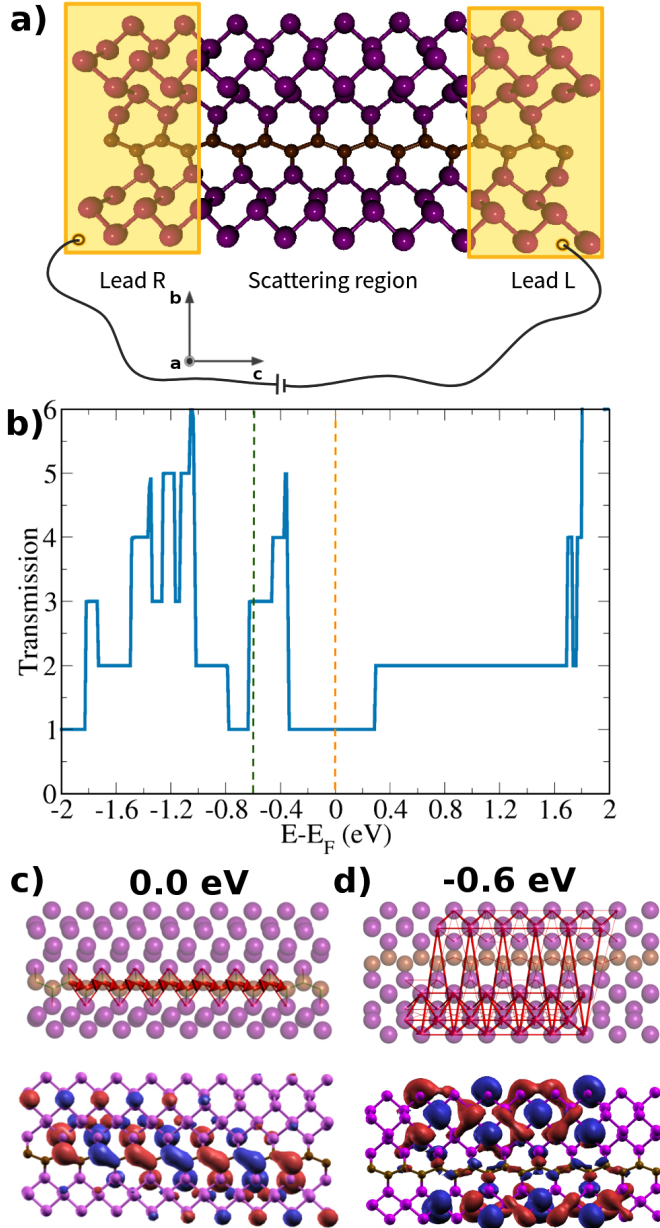


Fig. 4 (a) setup used for the electronic transports calculations along y-direction in the BP-8C configuration; (b) transmission coefficient and (c) local current density and wave-function at 0.0 and -0.6 eV. The red(blue) color represent positive(negative) values.

In order to assessing the nature of chemical bonds in the phos-

phorene, Figure 3a shows the total charge density along the pristine phosphorene sheet, where we can observed the covalent bonds character between the phosphours atoms.

Aiming to understanding the changes of the local charge density in the P atoms due to presence of the C-doped in the phosphorene sheet, we have determined charge density redistribution and possible charge transfer between C and P atoms using Bader analysis^{38,39}. Figures 3b-f show the charge density redistribution for different concentrations and/or configurations of the C-doped in the phosphorene. As the red(blue) color indicate the gain(lost) of electronic charge, we can note that for all C defects studied herein showed that C atoms gain charge, as expected due to valence of the C (4e) and P (5e) atoms. For Figure 3 we noted a charge gain and based on Bader charge density analysis^{38,39} it was around $4.1e$ per C atom, in accordance with redistribution picture. The same behavior is observed for Figures 3c, d, e and f, where C atoms present an electron gain and quantified by Bader analysis as 2.42, 2.59, 1.19 and 1.39 e per C atoms, respectively.

Next, we focus our attention to the electronic transport properties of the zigzag C-wire in the phosphorene (BP-8C). The electronic transport calculation was performed using the setup showed in Figure4-a. Note that the leads are building of the same structure of the scattering region. For the referred setup was considered the zigzag C-wire in the transport direction (c-direction). We chose this setup due to it shows metallic behavior in ΓY direction, for this purpose we pointed the carbon line atoms in c-direction. The zero bias transmission is depicted in Figure 4-b, where we note one electron channel from -0.3 to 0.3 eV, two for the energy range from 0.4 to 1.6 eV, and stairs channels from -1.0 to -0.4 eV. The zero bias transmission projection were also calculated for two specific energies (0.0 and -0.6 eV), which represent the electron probability between two sites. Figure 4-c shows the local current (upper panel) and its wave function (lower panel) for $E=0.0$ eV. We note that the electron probability is confined in the Carbon wire, as confirmed in the wave function localization. The p_z electrons from the Carbon wire atoms are responsible for this local current. Finally, we show in Figure 4-d the zero bias transmission projection for $E=-0.6$ eV, where the system has three electron channels from the transmission curve. We also note the electron probability projection are spread through the whole system, but at the carbon wire there is a small local current in comparison with the other part of the system. The wave function corroborate with the last finds showing a localized wave in C wires, but with small amplitude. For the Phosphorus part of the system the wave function is spread leading to different path ways for electron transmission. The key point here is the possibility to control the electron pathway through applied gate voltage. As an application the nanowire embedded in a semiconductor material could be used to connect two circuits in nanotransistors. Another possibility could be use this proposed material as metallic nanochannel or nanosensor of small gas molecules in the wire surroundings.

3 Conclusions

Based on DFT calculations, we have explored the structural and electronic properties, electronic transport properties, and the en-

energetic stability of the substitutionally C-doped phosphorene. Our results revealed that carbons defects in phosphorene sheet are energetically stable and ruled by exothermic process. We also observed that substitutional C-doped phosphorene sheet change its electric properties, i.e., a transition semiconductor to metallic was observed due to presence of the defects concentrations and geometric configurations. Finally, we verified for C defects in line the high anisotropic character of the electronic and transport properties of zig-zag compared to armchair interface.

Conflicts of interest

In accordance with our policy on Conflicts of interest please ensure that a conflicts of interest statement is included in your manuscript here. Please note that this statement is required for all submitted manuscripts. If no conflicts exist, please state that “There are no conflicts to declare”.

Acknowledgements

The authors acknowledge financial support from the Brazilian agencies CAPES, CNPq, FAPES/CNPq (05/2017) and the LNCC (SCAFMat2), CENAPAD-SP for computer time. WLS and RGA thank for financial support from CNPq (301648/2017-4 and 421227/2018-4) and (2535/2017-1 and 437182/2018-5), respectively.

Notes and references

- 1 E. S. Souza, W. L. Scopel and R. Miwa, *Physical Review B*, 2016, **93**, 235308.
- 2 A. J. Mannix, X.-F. Zhou, B. Kiraly, J. D. Wood, D. Alducin, B. D. Myers, X. Liu, B. L. Fisher, U. Santiago, J. R. Guest *et al.*, *Science*, 2015, **350**, 1513–1516.
- 3 B. Feng, J. Zhang, Q. Zhong, W. Li, S. Li, H. Li, P. Cheng, S. Meng, L. Chen and K. Wu, *Nature Chemistry*, 2016, **8**, 563.
- 4 R. Das, B. Rakshit, S. Debnath and P. Mahadevan, *Physical Review B*, 2014, **89**, 115201.
- 5 G. Moynihan, S. Sanvito and D. D. O’Regan, *2D Materials*, 2017, **4**, 045018.
- 6 F. A. de Souza, R. G. Amorim, J. Prasongkit, W. L. Scopel, R. H. Scheicher and A. R. Rocha, *Carbon*, 2018, **129**, 803–808.
- 7 V. Shukla, J. Walrha, N. K. Jena, A. Grigoriev and R. Ahuja, *The Journal of Physical Chemistry C*, 2017, **121**, 26869–26876.
- 8 N. Suvansinpan, F. Hussain, G. Zhang, C. H. Chiu, Y. Cai and Y.-W. Zhang, *Nanotechnology*, 2016, **27**, 065708.
- 9 H. Liu, A. T. Neal, Z. Zhu, Z. Luo, X. Xu, D. Tománek and P. D. Ye, *ACS nano*, 2014, **8**, 4033–4041.
- 10 J. Qiao, X. Kong, Z.-X. Hu, F. Yang and W. Ji, *Nature communications*, 2014, **5**, 4475.
- 11 X. Wang, A. M. Jones, K. L. Seyler, V. Tran, Y. Jia, H. Zhao, H. Wang, L. Yang, X. Xu and F. Xia, *Nature nanotechnology*, 2015, **10**, 517.
- 12 L. Li, J. Kim, C. Jin, G. J. Ye, D. Y. Qiu, H. Felipe, Z. Shi, L. Chen, Z. Zhang, F. Yang *et al.*, *Nature nanotechnology*, 2017, **12**, 21.
- 13 J. D. Wood, S. A. Wells, D. Jariwala, K.-S. Chen, E. Cho, V. K. Sangwan, X. Liu, L. J. Lauhon, T. J. Marks and M. C. Hersam, *Nano letters*, 2014, **14**, 6964–6970.
- 14 W. L. Scopel, E. S. Souza and R. Miwa, *Journal of Physics: Condensed Matter*, 2016, **29**, 075002.
- 15 G. Yang, S. Xu, W. Zhang, T. Ma and C. Wu, *Physical Review B*, 2016, **94**, 075106.
- 16 W. Hu, L. Lin, R. Zhang, C. Yang and J. Yang, *Journal of the American Chemical Society*, 2017, **139**, 15429–15436.
- 17 Y. Ren, F. Cheng, Z. Zhang and G. Zhou, *Scientific reports*, 2018, **8**, 2932.
- 18 X. Cai, C. Niu, Y.-Y. He, J. Wang, Z. Zhu, L. Zhang and Y. Jia, *Physical Chemistry Chemical Physics*, 2017, **19**, 28354–28359.
- 19 M. C. Watts, L. Picco, F. S. Russell-Pavier, P. L. Cullen, T. S. Miller, S. P. Bartus, O. D. Payton, N. T. Skipper, V. Tileli and C. A. Howard, *Nature*, 2019, **568**, 216.
- 20 X. Tian, L. Liu, Y. Du, J. Gu, J.-b. Xu and B. I. Yakobson, *Physical Chemistry Chemical Physics*, 2015, **17**, 31685–31692.
- 21 D.-T. Phan, I. Park, A.-R. Park, C.-M. Park and K.-J. Jeon, *Scientific reports*, 2017, **7**, 10561.
- 22 Y. Cai, G. Zhang and Y.-W. Zhang, *The Journal of Physical Chemistry C*, 2015, **119**, 13929–13936.
- 23 A. Hashmi and J. Hong, *The Journal of Physical Chemistry C*, 2015, **119**, 9198–9204.
- 24 L. Yang, W. Mi and X. Wang, *Journal of Alloys and Compounds*, 2016, **662**, 528–533.
- 25 J. P. Perdew, K. Burke and M. Ernzerhof, *Phys. Rev. Lett.*, 1996, **77**, 3865.
- 26 P. E. Blüchl, *Phys. Rev. B*, 1994, **50**, 17953.
- 27 G. Kresse and J. Furthmüller, *Comput. Mater. Sci.*, 1996, **6**, 15.
- 28 G. Kresse and J. Furthmüller, *Phys. Rev. B*, 1996, **54**, 11169.
- 29 H. J. Monkhorst and J. D. Pack, *Phys. Rev. B*, 1976, **13**, 5188.
- 30 J. M. Soler, E. Artacho, J. D. Gale, A. García, J. Junquera, P. Ordejón and D. Sánchez-Portal, *J. Phys.: Condens. Matter*, 2002, **14**, 2745.
- 31 M. Brandbyge, J.-L. Mozos, P. Ordejón, J. Taylor and K. Stokbro, *Phys. Rev. B*, 2002, **65**, 165401.
- 32 E. Artacho, D. Sánchez-Portal, P. Ordejón, A. Garcia and J. M. Soler, *Phys. Status Solid B*, 1999, **215**, 809.
- 33 Within the SIESTA code, the cutoff radius of the basis set (pseudoatomic orbitals) can be tuned by a single parameter, *energy shift*. For lower *energy shift* we have larger cutoff radii for the atomic orbitals, that is, the basis set has been improved. In the present work we have considered an energy shift of 0.10 eV to determine the radius cutoff of the pseudoatomic orbitals. Here we verify the convergence of our total energy results for an *energy shift* of 0.05 eV.
- 34 M. Paulsson and M. Brandbyge, *Transmission eigenchannels from nonequilibrium Green’s functions*, 2007, <https://link.aps.org/doi/10.1103/PhysRevB.76.115117>.
- 35 M. Brandbyge, J.-L. Mozos, P. Ordejón, J. Taylor and K. Stokbro, *Phys. Rev. B*, 2002, **65**, 165401.
- 36 Y. Zhao, J. Ning, X. Hu, J. Tu, W. Zou, X. Ruan, Y. Li, Y. Xu and L. He, *Applied Surface Science*, 2019, 144488.

- 37 W. Yu, Z. Zhu, C.-Y. Niu, C. Li, J.-H. Cho and Y. Jia, *Physical Chemistry Chemical Physics*, 2015, **17**, 16351–16358.
- 38 R. F. W. Bader, *Atoms in Molecules: A Quantum Theory*, Oxford University Press, New York, 1990.
- 39 W. Tang, E. Sanville and G. Henkelman, *J. Phys. : Condens. Matter*, 2009, **21**, 084204.